A&A 372, 281–290 (2001)
DOI: 10.1051/0004-6361:20010468

Astronomy & Astrophysics

SiO in G34.26: Outflows and shocks in a high mass star forming region

J. Hatchell[1,2], G. A. Fuller[1], and T. J. Millar[1]

[1] Astrophysics Group, UMIST, PO Box 88, Sackville Street, Manchester M60 1QD, UK
[2] Max-Planck-Institut für Radioastronomie, Auf dem Hügel 69, 53121 Bonn, Germany

Received 6 February 2001 / Accepted 26 March 2001

Abstract. We have looked for SiO emission as evidence of shocks in the high mass star formation region G34.26+0.15. JCMT, VLA and FCRAO observations show that SiO emission is widespread across the region. The SiO emission highlights a massive, collimated outflow and other regions where stellar winds are interacting with molecular clumps. As in other star forming regions, there is also SiO at ambient velocities which is related to the outflow activity. No strong SiO abundance enhancement was measured in either the outflow or the low velocity gas, though abundances up to 10^{-8} are possible if the SiO is locally enhanced in clumps and optically thick. SiO emission is not detected from the hot core itself, indicating either that SiO is not strongly enhanced in the hot core or that column densities in the region where grain mantle evaporation has taken place are low. In line of sight spiral arm clouds, we measure a SiO abundance of $0.4\text{–}2 \times 10^{-10}$, consistent with previous estimates for quiescent clouds.

Key words. stars: formation – ISM: abundances – ISM: G34.26+0.15 – ISM: jets and outflows – ISM: molecules – radio lines: ISM

1. Introduction

SiO is a good tracer of shocks in interstellar molecular clouds. Most silicon is locked up in dust grains, and when this is released through grain destruction and sputtering, SiO abundances in the gas phase can rise by several orders of magnitude. These enhancements are predicted by recent sputtering calculations (Schilke et al. 1997; May et al. 2000) and observed in protostellar outflows where shocks are known to occur (Avery & Chiao 1996; Ziurys & Friberg 1987).

In high mass star formation regions, SiO is a particularly useful tracer of molecular outflows. Molecular outflows in high mass star forming regions are common: Shepherd & Churchwell (1996) detected high velocity linewings in 90% of the regions they surveyed. For high mass sources, most of which lie in the Galactic plane, SiO has the advantage over CO (the outflow tracer most used for low mass sources) of being less confused by emission and absorption by unrelated molecular clouds. Partly for this reason, and partly because high mass sources are typically further away so equivalent outflows have smaller angular size, relatively few high mass outflows have been studied. Where outflows have been imaged, they are often detected in SiO (Ziurys & Friberg 1987; Shepherd et al. 1997; Cesaroni et al. 1999; Hunter et al. 1999). The disadvantage of using SiO to trace outflows is that its abundance is lower than CO so it only traces massive flows, and as the abundance varies over several orders of magnitude it cannot be used to estimate the outflow mass.

SiO may also trace shocks in hot cores. Hot cores are regions of hot, dense molecular gas in high mass star forming regions, characterised by high abundances of species which have a grain ice origin. The material released from the ices is processed in the hot, dense gas phase leading to high abundances of complex molecules. Column densities are high so even the less abundant species can be detected in hot cores. They are therefore excellent regions in which to investigate models of interstellar chemistry (e.g. Macdonald et al. 1996; Mehringer & Snyder 1996; Millar et al. 1997; Hatchell et al. 1998; Viti et al. 1999) and, through these, identify tracers of the conditions and evolution of the regions.

The grain evaporation is usually assumed to have a thermal origin but shocks are an alternative mechanism for removing ices (and more) from grains. The two scenarios lead to differences in the subsequent chemistry. In particular, the chemistry runs faster in shocks as the temperatures and densities are higher. Also, all species are evaporated instantaneously in a shock, whereas thermal evaporation may bring ices off in layers (Viti & Williams 1999). Thus it is important to know if hot cores are shocked in order to understand the chemistry and the evolutionary timescales.

Send offprint requests to: J. Hatchell,
e-mail: hatchell@mpifr-bonn.mpg.de

In this paper we present SiO observations of G34.26+0.15, a widely studied high mass star forming region at a distance of ∼4.0 kpc. This region consists of a number of ultracompact HII (UCHII) regions (Wood & Churchwell 1989; Gaume et al. 1994; Fey et al. 1994) and other infrared sources (Campbell et al. 2000). In the rest of the paper we use the notation of Gaume et al. (1994) to label the UCHII regions: C is the cometary UCHII; A and B are unresolved UCHII to the southeast and northeast of C respectively; and D is a shell HII region to the southeast (see labelling in Fig. 6). The hot molecular core, which lies at the head of UCHII C (Garay & Rodriguez 1990; Watt & Mundy 1999), is one of the richest known molecular line sources (Churchwell et al. 1992; Macdonald et al. 1996; Millar et al. 1995). There are associated H_2O, CH_3OH and OH masers (Fey et al. 1994; Caswell et al. 1995, 1995; Hofner & Churchwell 1996; Forster & Caswell 1999). The hot core and UCHII regions are embedded in an extended molecular cloud (Matthews et al. 1987; Scoville et al. 1987; Carral & Welch 1992; Heaton et al. 1985, 1993).

In Sect. 2 we describe the observations. In the following sections we present our results on outflows, ambient emission, the hot core and foreground molecular clouds (Sects. 3.1–3.4). Finally, our conclusions are in Sect. 4.

2. Observations

2.1. VLA observations

We observed G34.26 in the SiO 43 GHz $J = 1$–0 rotational transition using the Very Large Array (VLA)[1] in December 1997. Simultaneous observations of the $NH_3(4,4)$ line were carried out using the remaining non-Q-band antennas. The observing parameters are given in Table 1.

The data were reduced using AIPS. Continuum subtraction was done in the UV plane using the line-free velocity ranges 33–40 and 87–93 km s^{-1}. The 7 mm continuum was self-calibrated and the solutions applied to the spectral line data, which (following initial channel maps) were then imaged, averaging over certain velocity ranges and CLEANed. Because of the weakness of the SiO emission, natural weighting was used for maximum signal-to-noise ratio. For the final images, the UV data were taper weighted, resulting in a final resolution of $3.4'' \times 3.1''$ (at position angle $-72°$).

2.2. JCMT observations

JCMT[2] observations of SiO $J = 5$–4, 6–5 and 8–7 were made in May 1997 using the facility common user receivers A2 and B3. Frequencies and observing parameters are given in Table 2. All spectra are converted to the $T_{\rm MB}$ scale via the main beam efficiency $\eta_{\rm MB}$ as given in Table 2. Single spectra of all three transitions were observed towards the UCHII region at $18^{\rm h}50^{\rm m}46\overset{\rm s}{.}1$ $01°11'12''$ (B1950). In addition, SiO $J = 5$–4 was observed towards a position $(0, 20'')$. Observations were made in dual sideband mode with sideband separations of 3 and 8 GHz for receivers A and B respectively. For the $J = 5$–4 and 8–7 observations, to disentangle main and image sideband lines the SiO lines were placed alternately in the upper and lower sideband. Observations were position switched to an position offset $(-80'', -410'')$ in RA and Dec.

Table 1. Observing parameters at the VLA.

Array configuration	D
Observing frequency	43.4238 GHz
Number of Q-band antennas	13
Number of channels	64
Channel bandwidth	195.3 kHz
Velocity resolution	2.7 km s^{-1}(1)
Total velocity coverage	86 km s^{-1}
Primary beam $FWHM$	$62''$
Largest angular scale	$43''$
Synthesised beam $FWHM$	$2.4'' \times 1.9''$
Source	G34.26+0.15(2)
Primary flux calibrator	3C 286
Bandpass calibrator	1741-038
Phase calibrator	1849+005(3)

(1) After Hanning smoothing.
(2) $18^{\rm h}50^{\rm m}46\overset{\rm s}{.}1$ $+01°11'12''$(B1950).
(3) $18^{\rm h}49^{\rm m}13\overset{\rm s}{.}573$ $+00°31'53\overset{''}{.}34$ (B1950) (Fey et al. 1991).

Table 2. Observing parameters at JCMT.

Transition	5–4	6–5	8–7
Frequency/GHz	217.1050	260.5180	347.3306
Receiver	A2	A2	B3
Integration time/mins	12, 15	8	4, 8
Main beam efficiency $\eta_{\rm MB}$	0.79	0.79	0.62
Beam $FWHM$ $\theta_{\rm B}$	$21''$	$17''$	$13''$

2.3. FCRAO observations

A $6' \times 6'$ half-beam-sampled map of SiO $J = 2$–1 was made in December 2000 with the FCRAO 14 m using the 16-pixel SEQUOIA focal plane array. The integration time per position was 2 min 40 s and the angular resolution is $55''$ at the 2–1 frequency of 86.8470 GHz. All spectra were corrected for the main beam efficiency of 0.46.

3. Results

All three SiO transitions ($J = 5$–4, 6–5 and 8–7) were detected at the JCMT. The spectra are shown in Fig. 1.

[1] The VLA is part of the National Radio Astronomy Observatory, a facility of the US National Science Foundation operated under cooperative agreement by Associated Universities, Inc.

[2] The James Clerk Maxwell Telescope is operated by the Joint Astronomy Centre on behalf of the Particle Physics and Astronomy Research Council of the UK, The Netherlands Organisation for Scientific Research, and the National Research Council of Canada.

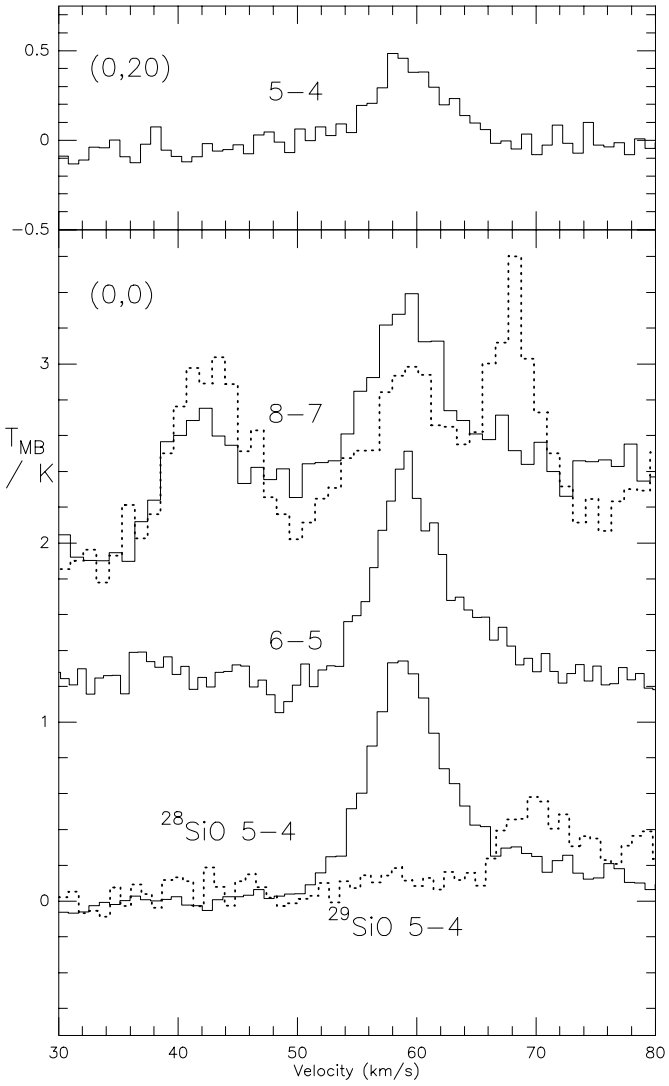

Fig. 1. JCMT SiO spectra centred on the UCHII region C. See Sect. 2 for description of dual sideband spectra. Bottom to top: ^{29}SiO 5–4 (dotted) and SiO 5–4 (solid); SiO 6–5 (solid); and SiO 8–7 LSB (solid) and USB (dotted). The lines in the ^{29}SiO spectrum at >70 km s^{-1} are attributed to $^{13}CH_3CN$.

The line peaks at velocities between 58 and 60 km s^{-1} with a $FWHM$ of 9 km s^{-1}, as do other molecular species in G34.26 (eg. Hatchell et al. 1998). There is clearly a redshifted wing in the 5–4 and 6–5 spectra. The 8–7 line is blended with lines from other species in both the main and image sidebands. Peak intensities are of order 1 K. At a position 20″ to the north, SiO 5–4 was also observed and detected with a similar line shape and a peak strength of 0.5 K.

VLA emission maps are shown in Fig. 2. The 7 mm continuum emission shows the extended cometary ultracompact HII region C including tails to the west and southwest, and also the UCHII B, which is seen as an extension to the northeast on UCHII C, and UCHII A to the southeast. At ambient velocities (around 58 km s^{-1}), widespread SiO emission was detected over a region approximately 1′ × 20″. To the northwest of the UCHII regions, blueshifted emission forms an elongated structure. Strong redshifted and blueshifted emission are seen to the southeast of the UCHII.

The VLA also detected strong SiO absorption in front of the UCHII regions at velocities 60, 53 and 27 km s^{-1} (Fig. 3).

The FCRAO observations are sensitive to large scale emission components which could be resolved out at the VLA, and the 2–1 transition traces similarly low-excitation gas. However, the SiO emission is confined to a region about an arcminute across (Fig. 4).

3.1. A massive outflow

At blueshifted velocities, there is a collimated SiO emission extending to the northwest of G34.26 (Fig. 2c), which we interpret as tracing a molecular outflow. The direction and velocity of this high velocity feature agree with the outflow discovered in ^{13}CO by Matthews et al. (1987). This molecular outflow is not well known. Interferometric observations of ^{13}CO and CH_3OH centred on the hot core do not trace it, possibly due to limited spatial coverage.

The blueshifted NW SiO outflow reaches velocities of at least 13 km s^{-1} from ambient (to 45 km s^{-1}). In the VLA maps it appears to end 33″ or 0.63 pc from the UCHII position. The VLA emission could underestimate the true extent of the outflow as the half power point of the VLA primary beam is only 30″, but the large-scale FCRAO map peaks only 20″ to the northwest of the UCHII and shows that the true extent of the outflow is at most an arcminute (Fig. 4). The ^{13}CO outflow peaks 1′ from the UCHII (Matthews et al. 1987). The dynamical age of the outflow is then 10^5 years (with no inclination correction).

3.1.1. SiO abundance in the outflow

In other outflows where SiO has been detected, there is evidence for SiO abundance enhancements of a factor of 10^3: $X(\mathrm{SiO}) = 5 \times 10^{-7}$ in L1157 and 2×10^{-7} in Orion IRc2 (Avery & Chiao 1996; Ziurys & Friberg 1987). Here we look for evidence of SiO abundance enhancements in the G34.26 outflow.

From the VLA data, a strict column density lower limit for SiO in the outflow (assuming LTE and optically thin emission) is $N(\mathrm{SiO}) \geq 1.8 \times 10^{13}$ cm^{-2}, over the velocity range 48–57 km s^{-1}. A more realistic estimate assuming the outflow is warm, ∼50 K, is 1.6×10^{14} cm^{-2}. Integrating over the outflow area, the total number of SiO molecules is 1×10^{50}. The same number is reached from the FCRAO data, which shows that little or no emission is being resolved out by the VLA.

For comparison, the mass of the ^{13}CO outflow is 150 $M_\odot$ (Matthews et al. 1987) giving a SiO abundance of $X[\mathrm{SiO}] = 1 \times 10^{-9}$.

The H_2 column density can be estimated from 450 micron observations with SCUBA (Thompson, priv. comm.).

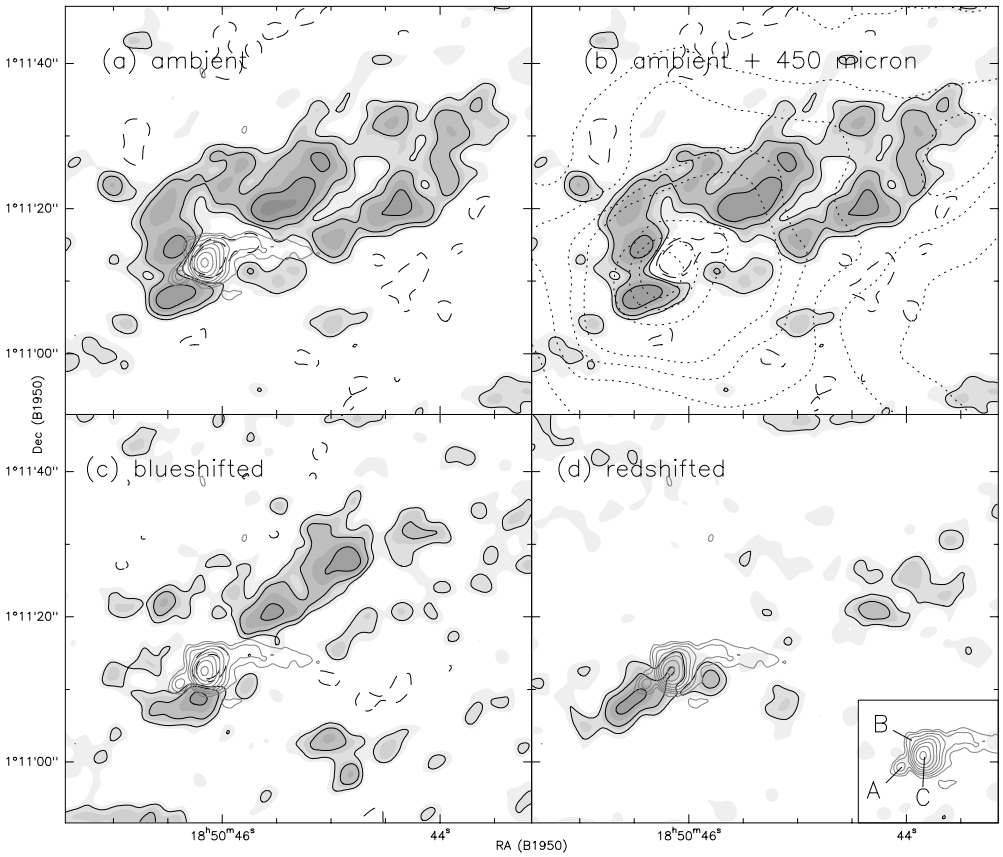

Fig. 2. SiO $J = 1$–0 VLA images (greyscale and thin black contours), reconstructed with a $3.4'' \times 3.1''$ beam, overlaid with 7 mm continuum contours (grey). Maps are: **a)** ambient velocities (55–62 km s^{-1}); **b)** as **a)** with 450 μm contours at $8''$ resolution overlaid (dotted); **c)** blueshifted velocities (51–57 km s^{-1}); and **d)** redshifted velocities (65–78 km s^{-1}); the inset shows the labelling of UCHII A, B and C. Contours for the 7 mm continuum are from 20 mJy/beam increasing by a factor of 2 each contour; for the emission, -20 and -10 mJy/beam then from 5 mJy/beam increasing by factors of 2; for the 450 μm data, 10–50 Jy/beam by 10 Jy/beam, then 100–300 Jy/beam by 50 Jy/beam. The noise level on the maps is 5.0, 3.0 and 4.4 mJy/beam for ambient, redshifted and blueshifted emission respectively.

These show dust emission to the northwest extended in the same direction as the outflow (Fig. 2b). Assuming a dust temperature of 20 K and standard interstellar dust opacities (Draine & Lee 1984), column densities from the 450 μm data are $\sim 10^{24}$ cm^{-2}, giving a SiO abundance of $\sim 10^{-10}$. These values become $\sim 10^{23}$ cm^{-2} and $X(\mathrm{SiO}) \sim 10^{-9}$ if icy coagulated dust (Ossenkopf & Henning 1994) and a temperature of 50 K are assumed.

Further estimates of the outflow mass that might be expected comes from the correlations between between core and outflow mass (Beuther & Schilke, priv. comm., based on a sample of 69 objects) and between outflow force and source bolometric luminosity (Cabrit & Bertout 1992). Taking a core mass of 4000 $M_\odot$ from CO isotopes, (Hatchell et al. 1998), Beuther & Schilke predict an outflow mass of $\sim$150 $M_\odot$ to with a factor of three uncertainty. This agrees with what was detected in ^{13}CO. Using Eqs. (2) and (4) of Cabrit & Bertout (1992) with $V = 13$ km s^{-1} and $R = 0.63$ pc, and the luminosity of G34.26 which is $L_{\mathrm{FIR}} = 10^{5.672}$ $L_\odot$ (Churchwell et al. 1990), the predicted outflow mass is 10^3 $M_\odot$. (We are extrapolating to masses/luminosities slightly beyond Cabrit & Bertout's sample of sources up to $10^{5.3}$ $L_\odot$.) As the luminosity comes from more than one source, this will overestimate the outflow mass. Taking 10^3 $M_\odot$ for the outflow mass, $X[\mathrm{SiO}] \simeq 10^{-10}$.

SiO abundance estimates for the outflow thus range from 10^{-10}–10^{-9}. These are at most a factor of 10 enhanced over SiO abundances in diffuse clouds of 2×10^{-11}–2×10^{-10} (Lucas & Liszt 2000) and in spiral arm clouds, $\sim 10^{-10}$ (Greaves et al. 1996). In this paper we calculate 0.4–2×10^{-10} from foreground absorption in front of G34.26 (Sect. 3.4).

These abundance estimates provide direct evidence for only slightly higher SiO abundances in the outflow than in quiescent clouds. Yet we expect SiO in the outflow to be strongly enhanced as a result of shock activity. In fact moderate abundance enhancements up to $X(\mathrm{SiO}) \sim 10^{-8}$ are still consistent with the data. The above SiO column density estimates assume that the SiO is optically thin, whereas in fact it may well be clumpy and optically thick. The ^{29}SiO observations place a limit on the optical depth in ^{28}SiO. In Sect. 3.2 we show that in the ambient velocity material the $J = 5$–4 optical depth could

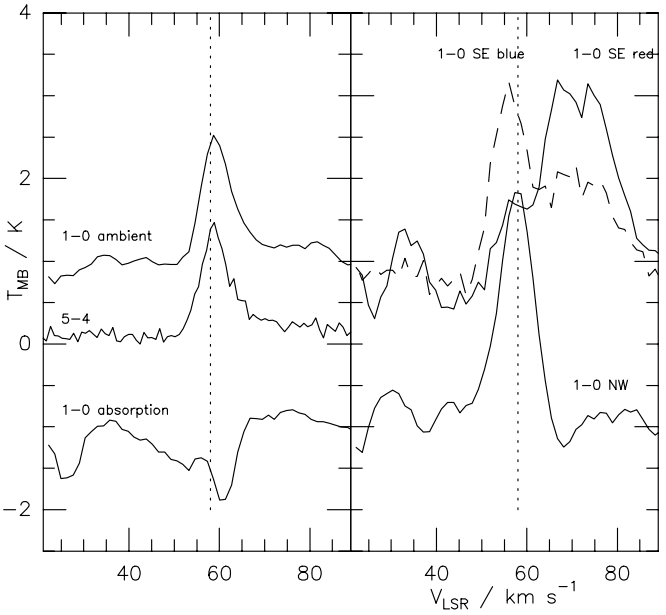

Fig. 3. SiO spectra integrated over various regions. All spectra are SiO $J = 1$–0 unless otherwise indicated. Left, top to bottom: Ambient emission over entire region; JCMT $J = 5$–4; absorption spectrum over UCHII region C (divided by 10). Right, top to bottom: spectra integrated over the blueshifted and redshifted gas to the southeast; and the northwest outflow. The VLA spectra are converted from Jy to K using $T_{\rm MB} = \frac{c^2}{2k_{\rm B}\lambda^2\Omega_{\rm B}}\left(\frac{\Omega_{\rm B}}{\Omega}\right)S$ or $\left(\frac{T_{\rm MB}}{\rm K}\right) = 206\left(\frac{\Omega_{\rm B}}{\Omega}\right)\left(\frac{S}{\rm Jy}\right)$.

be as high as 2 and column densities $\sim 10^{15}$ cm^{-2}. For the higher velocity outflow material, optical depths could also be of this order, in which case SiO abundances of $\sim 10^{-8}$ would indicate moderate enhancements over quiescent clouds. We think that clumpy, optically thick SiO can explain much of the apparent lack of SiO enhancement in the outflow. However, strong abundance enhancements ($X(\mathrm{SiO}) > 10^{-7}$) are ruled out by the observations, suggesting that the SiO is produced either in slow shocks (<30 km s^{-1}) which do not destroy grain cores, or that the outflow has aged and SiO partially depleted due to accretion and chemical processing (see Sect. 3.2).

A better estimate of the SiO abundance enhancement could be obtained from high resolution SiO observations in a higher excitation line which would trace the warm outflow material – with an excitation energy of just 2.1 K, the 1–0 line is not sensitive to warm gas. Observations of a high-J CO or ^{13}CO transition (to avoid problems with foreground absorption) at similar resolution would provide a more reliable estimate of the H_2 column density on similar scales to the SiO.

In addition to the northwest outflow, there is high velocity SiO to the southeast of the UCHII regions (Figs. 2c and d). This emission has blueshifted, ambient and redshifted velocity components and is localised to the region south of UCHII C. Watt & Mundy (1999) detected ^{13}CO and C^{18}O clumps in a similar region. This SiO may be evidence for interaction of winds, perhaps from UCHII A (southeast), with these molecular clumps. The H_2O masers to the southeast of the hot core all show blueshifted components and could be associated with the blueshifted SiO (Hofner & Churchwell 1996).

3.1.2. The outflow driving source

UCHII B (to the northeast) is a deeply embedded and therefore young star: our absorption spectra show that the SiO optical depth due to local molecular material in front of B is 15 times more (at 0.7) than in front of the cometary UCHII C (see Sect. 3.4). The corresponding H_2 column density for all but the highest SiO abundances ($X(\mathrm{SiO}) < 10^{-8}$) is enough to explain the mid-infrared (8.0–20.6 μm) non-detection of this source (Campbell et al. 2000). In low mass star forming regions it is the embedded sources which drive molecular outflows. UCHII B is therefore a strong candidate for the outflow powering source.

Source B also has the spectral index of a stellar wind (Gaume et al. 1994). Winds from UCHII B may be responsible for the velocity gradients and large linewidths in the UCHII region, which also has blueshifted gas to the north, and the ionised tails on the UCHII region (Gaume et al. 1994; Campbell et al. 2000). B may also be shocking the molecular clump to its east (Sect. 3.2) and disrupting the molecular hot core, which also shows velocity gradients (Watt & Mundy 1999; Akeson & Carlstrom 1996; Heaton et al. 1993; Carral & Welch 1992).

If the cometary UCHII region C were driving the outflow, one would expect the tails of ionised gas to outline the outflow cavity. This is clearly not the case and rules against C as the source of the outflow. The axis of the northwest outflow lobe also suggests that the UCHII ionising source is not driving the outflow. UCHII region B, the hot core, or source A lie more along the outflow axis, although the clumpy nature of the SiO emission prevents an exact determination.

The counterpart of the blueshifted NW outflow could be found to the east of source B, where there is strong SiO emission at ambient velocities on the eastern side of the C^{18}O core (Fig. 2a). If this is the counterpart, then it is confined by the high density ambient material into which it is being driven.

3.2. Widespread SiO emission

The VLA observations show widespread SiO emission at the ambient velocity of 58 km s^{-1} (Fig. 2a). There is clearly emission to the northwest, north and east of the radio continuum at ambient velocities. The northwest emission is more extended than the corresponding high velocity gas, with additional components to the north and south of the outflow.

The JCMT observations also show evidence for widespread SiO emission at ambient velocities. The JCMT spectra centred on the UCHII also show emission peaking at 58 km s^{-1}, as does a spectrum averaged over the

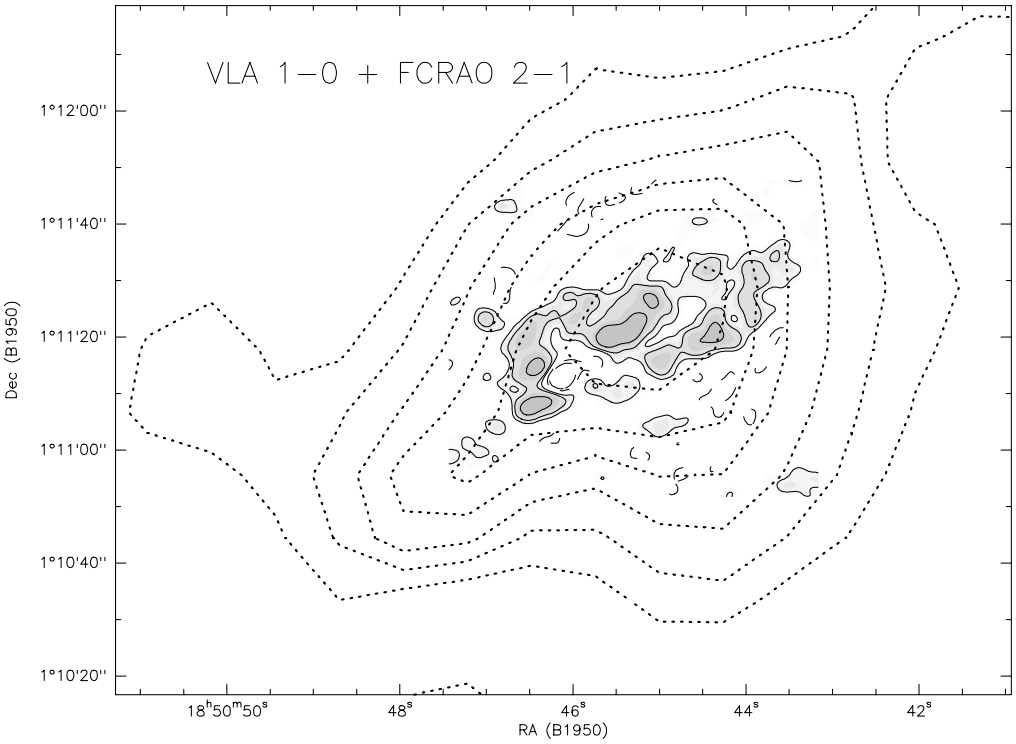

Fig. 4. Contours of SiO $J = 2$–1 emission at $55''$ resolution superimposed on SiO $J = 1$–0 emission at ambient velocities (greyscale). Contour levels for the 2–1 are every 0.25 K km s^{-1} from 0.5 K km s^{-1}, and for the 1–0 the same as Fig. 2.

northwest emission seen by the VLA (Fig. 3). Ambient velocity gas rather than high velocity gas dominates the spectrum, although the SiO $J = 5$–4 and higher J lines are wide, $\sim$9 km s^{-1}, and show a redshifted wing (due to the southeast outflow). Furthermore, JCMT spectra at an offset of ($0''$, $20''$) also show SiO at the same velocity (Fig. 1). This offset emission is only a factor of 3 less strong than at the central position. SiO emission close to the radio continuum peak can only account for $\sim$1/3 of the line strength at ($0''$, $20''$) (the JCMT beam $FWHM$ is $21''$ at 217 GHz).

The FCRAO spectra are also dominated by emission at around 58 km s^{-1}, although the SiO $J = 2$–1 clearly peaks in the direction of the outflow.

3.2.1. The origin of the ambient velocity SiO

Although SiO detections are often associated with shock enhancement, the molecular column densities in G34.26+0.15 are so high that we must consider if we could be detecting SiO at quiescent cloud abundances.

From the location of the SiO emission, this seems unlikely. Much of the SiO detected at ambient velocities lies in regions where high velocity gas is also detected – to the northwest, and to the southeast – suggesting that it is related to the outflow activity.

Comparing the distribution in SiO emission with the large scale ammonia (1, 1) and (2, 2) maps (Heaton et al. 1985) and the dust continuum emission at 850 and 450 μm (Fig. 2b), which are similar and both trace the total column density, the SiO only traces the northwest extension to the molecular cloud and not the southwest, although this has similar total column density. Particularly the FCRAO data show SiO peaking $20''$ to the northwest, rather than at the continuum core. This is consistent with some enhancement of SiO towards the northwest extension, though a factor of 10 over ambient cloud abundances would be enough enhancement to explain the detection of one part of the cloud but not the other, as neither the VLA or FCRAO detections have high signal-to-noise ratios.

The SiO to the northeast and southwest of the northwest outflow has no detectable high velocity component. It could be the slowed remnants of an earlier wind episode or an indication that the outflow lies nearly in the plane of the sky. The southeast SiO does not trace the high column density clumps traced by C^{18}O or ^{13}CO (Watt & Mundy 1999), but lies further to the southeast, and has redshifted and blueshifted components, so this feature is clearly not simply a quiescent clump with sufficient column density to be detected in SiO but may be the result of the interaction of winds from UCHII A with these clumps. The situation to the northeast is not so clear. The SiO lies at the north end of the C^{18}O clump (Watt & Mundy 1999), and has no redshifted or blueshifted component, and so may just be tracing ambient gas, or alternatively an interaction between the C^{18}O clump and a wind from UCHII B that lies in the plane of the sky.

From the morphology and kinematics, much of the SiO at ambient velocities is associated with outflows and winds, and it is likely that the remainder of the SiO has

Table 3. Beam averaged column density lower limits from each SiO transition.

transition	E_U/k K	$\int T_{MB}\,dv$ K km s^{-1} (2)	N_{min} $\times 10^{13}$ cm^{-2}
1–0	2.1	7(1)	1.6
5–4	31.3	11	1.5
6–5	43.8	12	1.5
8–7	75.0	13(3)	1.6

(1) SiO 1–0 emission integrated over $\Omega = 950''^2$ of ambient emission in Fig. 2, in Kelvin using the conversion of Fig. 3.
(2) For the JCMT detections, from Gaussian fits. Direct calculation of the integrated intensity from adding spectral channels gives values ∼10% bigger.
(3) The $J = 8$–7 line is blended with other transitions so this value may overestimate the true integrated intensity.

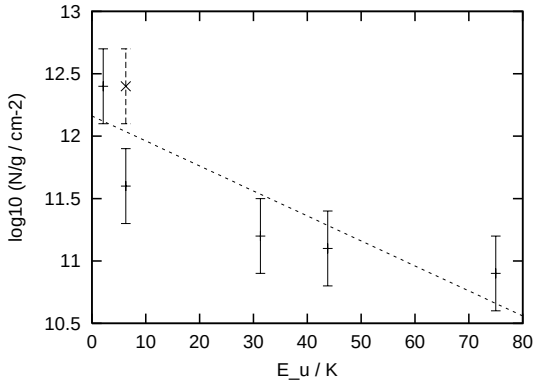

Fig. 5. Rotation diagram for SiO. The FCRAO data is plotted twice, as a solid errorbar assuming that the source uniformly fills the FCRAO beam, and as a dashed point corrected to the same beam size as SiO 5–4 at JCMT, assuming a compact source.

a similar origin. If this is the case then we might expect abundance enhancements in SiO over quiescent cloud values, as is seen in other outflows and predicted from shock models.

The critical densities for the SiO transitions are high, ranging from 1.3×10^5 cm^{-3} for $J = 1$–0 to 6.4×10^6 cm^{-3} for $J = 8$–7. Although central densities in G34.26 are thought to reach 10^7 cm^{-3}, densities have fallen to $\sim 10^5$ cm^{-3}, insufficient to thermalise SiO, at $10 - 20''$ from the source, where much of the SiO emission lies (Garay & Rodriguez 1990; Strong-Jones et al. 1991; Hatchell et al. 1998; Hofner et al. 2000). Yet the $J = 8$–7 line is similar in strength to the lower excitation lines, whereas for subthermal population at a density of 10^5 cm^{-3} it should be ten times weaker. To explain the JCMT-observed line intensities requires that the SiO emission originates from clumps with densities approaching the $J = 8$ critical density of 6.4×10^6 cm^{-3}, and that LTE is a reasonable approximation to the excitation.

A rotation diagram is shown in Fig. 5. This assumes that the SiO transitions are all tracing the same material, and that they are optically thin and in LTE. The results are $T = 22 \pm 6.2$ K and the beam averaged column density $N(\mathrm{SiO}) = 3.0 \pm 0.8 \times 10^{13}$ cm^{-2}. The rotation diagram is not wholly reliable because firstly, the amount of $J = 1$–0 resolved out is unknown although small (from comparison with the FCRAO $J = 2$–1 data), and secondly, the beam filling factors for the different JCMT beams may be different depending on the distribution of the emission, and thirdly, the $J = 8$–7 line is a blend with other lines so its individual column density has large uncertainties. The uncertainties quoted on the temperature and column density are assuming 50% calibration uncertainties on each line. This is overgenerous for instrumental calibration uncertainty but partly takes into account the other uncertainties. The FCRAO results are shown on the diagram but were not included in the fit because of the large uncertainty in the beam filling factor compared to the higher spatial resolution data from JCMT and the VLA.

Lower limits calculated from individual transitions, assuming LTE and optically thin emission, are consistently 1.5–1.6×10^{13} cm^{-2} (Table 3). These are calculated from

$$N_{\mathrm{min}} = \left(\frac{3\epsilon_0 k_{\mathrm{B}}}{2\pi^2}\right)\frac{1}{S\mu^2\nu}Q(E_{\mathrm{U}}/k_{\mathrm{B}})e \qquad (1)$$

where S is intrinsic line strength; μ dipole moment; ν frequency; $Q(E_{\mathrm{U}}/k_{\mathrm{B}})$ the rotational partition function calculated at the line upper state excitation energy; and the remaining symbols are the usual physical and mathematical constants.

An alternative explanation for the similar SiO line intensities in all four bands is that the lines (particularly 5–4 and 6–5) are optically thick. ^{28}SiO is optically thick in Orion, Sgr B2 and Sgr A (Penzias 1981). Limits on the ^{28}SiO optical depth in G34.26 come from limits on the ^{29}SiO line strength. In G34.26, ^{29}SiO 5–4 was possibly detected at 214.385 GHz: Fig. 1 shows that there is a plateau of emission around this frequency (the lines at >70 km s^{-1} are attributed to $^{13}CH_3CN$). The level of this emission is 0.15 K, with a 3σ upper limit of 0.23 K. Compared to a 1.3 K ^{28}SiO 5–4 line, the optical depth in ^{28}SiO 5–4 is ∼2 (at most 3.5).

An ^{28}SiO 5–4 optical depth of 2 corresponds to a source-averaged column density of 0.4–1.1×10^{15} cm^{-2} assuming $[^{28}\mathrm{SiO}/^{29}\mathrm{SiO}] = 20$ and LTE at 20–50 K. (The terrestrial ^{28}SiO/^{29}SiO ratio is 19.6 and Penzias (1981) give ratios of 10–20 in the interstellar medium.) We note that this solution with optically thick 5–4 and 6–5 lines predicts less 1–0 emission than is observed, by factors of 2 and 8 at 20 and 50 K respectively. A factor of 2 may easily be explained by the distribution of the 1–0 emission compared to the JCMT beam. From the distribution of the emission detected at the VLA the filling factor for the JCMT is $\eta \sim 0.5$ but a factor of 8 is hard to explain, especially as there may be additional 1–0 emission which is resolved out with the VLA, so we prefer the 20 K solution.

From dust continuum and CO isotopomers, the molecular hydrogen column density on similar scales to the SiO lies in the range $N(\mathrm{H_2}) = 0.7$–4×10^{24} cm^{-2} (Hatchell et al. 1998, 2000; Hofner et al. 2000). From the

above estimates for the SiO column density ($3.0 \pm 0.6 \times 10^{13}$ cm^{-2} if optically thin, at most 1.1×10^{15} cm^{-2} if optically thick) we calculate

$$X(\mathrm{SiO}) = 8 \times 10^{-12}\text{–}2 \times 10^{-9}, \quad (2)$$

compared to spiral arm cloud abundances of 10^{-10}.

The SiO abundance in the widespread ambient emission is therefore consistent with the abundances seen in quiescent molecular clouds, and at most enhanced by a factor of 10, if X(SiO) lies at the upper end of the calculated range (optically thick). The low abundances are a somewhat surprising result if the SiO traces the interaction of winds, as suggested by the kinematics and morphology.

Codella et al. (1999) also detected low velocity, low abundance SiO in several outflow regions and propose that the low velocity SiO is tracing material that was once shocked, compressed and accelerated in outflows but has since slowed down. The low SiO abundances are then explained by either conversion to SiO_2 or direct accretion onto grains on timescales of 10^4 years (Bergin et al. 1998; Pineau des Forêts et al. 1997). Alternatively, the SiO may be tracing slow shocks which do not significantly sputter grains: velocities must be less than 30 km s^{-1} for our observed column densities, from sputtering calculations (May et al. 2000; Schilke et al. 1997). If slow shocks are producing the lower velocity SiO to the northwest of the UCHII they could be due to a less collimated component to the wind driving the northwest outflow.

3.3. SiO: Evidence for shocks in the hot core?

In this section we ask if there is there any evidence for SiO in the hot core itself. Hot cores including G34.26 show high abundances of grain evaporated species and their daughter products. The mechanism for removing these molecules from grain ices is widely assumed to be thermal evaporation but shock removal is an alternative which has not yet been ruled out. High abundances of SiO in the hot core would indicate that shocks are important in removing grain mantles.

The hot core as traced by NH_3 and CH_3CN lies at the head of the UCHII region, between UCHII regions A, B and C. Figure 6 shows the relationship between these components, with the hot core traced by the $NH_3(4,4)$ hyperfine line. The hydrogen column density in the hot core on similar scales to the VLA synthesised beam is at most 8×10^{24} cm^{-2} and more probably 2×10^{24} cm^{-2}, considering an upper limit from the dust emission and values derived for the C^{18}O core to the east (Watt & Mundy 1999). If the SiO abundance in the hot core is the same or greater than the abundance in spiral arm and diffuse clouds, $X(\mathrm{SiO}) \sim 10^{-10}$, then the SiO column density in the hot core would be 10^{14}–10^{15} cm^{-2} or more.

If the hot core were in front of the UCHII then the column density of SiO in absorption would be expected to reflect the column density of the hot core. The measured SiO absorption column density is 6×10^{12} cm^{-2} (Sect. 3.4

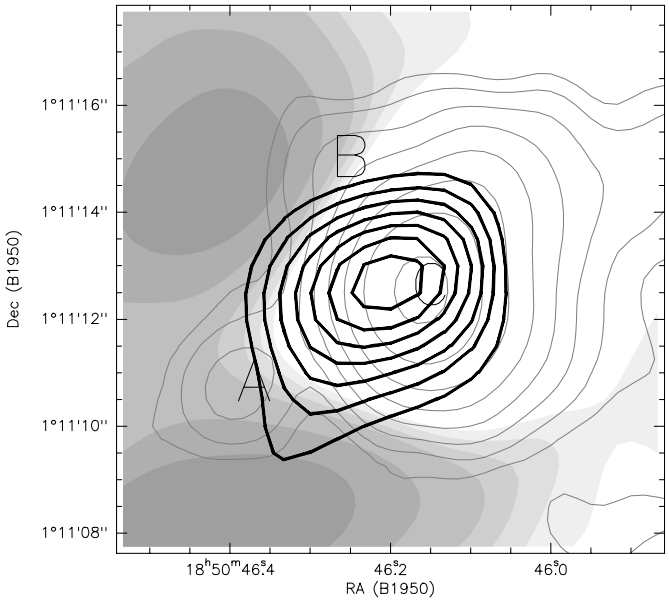

Fig. 6. $NH_3(4, 4)$ integrated hyperfine emission superimposed on SiO $J = 1$–0 emission at ambient velocities (greyscale) and 7 mm continuum contours (grey). Contour levels for the NH_3 are every 5 mJy/beam from 1 mJy/beam, and for the 7 mm continuum and emission as in Fig. 2.

so the hot core cannot lie in front of the cometary UCHII region. This confirms the result from NH_3 (Heaton et al. 1989). Therefore we would expect to see the hot core in emission in SiO, if at all.

In emission at hot core temperatures of 100 K, if the emission were thermalised, a SiO column density of 10^{15} cm^{-2} would produce a line strength only 1–2 times the rms noise on our maps. This would not be detectable, even without the confusion of the strong absorption in front of the UCHII region. However, we should certainly be able to detect SiO column densities of 10^{16} cm^{-2} in the hot core or abundances of 10^{-8}, if the C^{18}O column density is representative for the hot core. The fact that we do not see any SiO in emission at the hot core position could indicate that SiO is not strongly enhanced in the hot core, and that the hot core is not sufficiently shocked to destroy grain cores.

An alternative explanation which may apply in G34.26 is that the column density in the hot core itself could be very low, a few times 10^{23} cm^{-2}, as Watt & Mundy (1999) suggest to explain the lack of C^{18}O emission coincident with the NH_3. In this case the SiO abundance could be as high as 10^{-8} in the hot core region and still not detected by the VLA, although it would contribute to the higher excitation transitions observed at JCMT. This explanation is possible for G34.26 where the hot core may be externally heated by shocks and radiation from the direction of the UCHII region, rather than being a further site of star formation. SiO abundances of 10^{-8} could be produced by low velocity shocks which remove grain ice mantles, assuming a small fraction of all Si is in the ice, without disrupting the grain cores,which require higher velocity

Table 4. SiO peak optical depths, column densities (per unit velocity) and abundances from absorption components.

$v_{\rm peak}$ km s^{-1}	$\tau_{\rm peak}$	N(SiO) $\times10^{11}$ cm^{-2} (km s^{-1})$^{-1}$	N(HCO$^+$)$^{(1)}$ $\times10^{21}$ cm^{-2} (km s^{-1})$^{-1}$	[SiO]/[HCO$^+$]	X(SiO)
60	0.045	1.8	–	–	–
53	0.026	1.1	3.0	0.018	4×10^{-11}
27	0.031	1.3	0.55	0.12	2×10^{-10}

(1) Carral & Welch (1992).

shocks (Schilke et al. 1997). High resolution observations of high excitation transitions of SiO are required to determine if the G34.26 hot core is shocked or not.

3.4. SiO abundances in foreground clouds

The SiO spectra towards the UCHII show absorption features at 60, 53 and 27 km s^{-1} (Fig. 3). These features were also previously noted in HCO$^+$ absorption by Carral & Welch (1992). They concluded that the 60 km s^{-1} gas was local to G34.26 but the 53 and 27 km s^{-1} components were due to foreground molecular clouds. Comparing the SiO optical depth in these features with that from HCO$^+$ gives an estimate of the SiO abundance in these foreground molecular clouds.

We measured the continuum and the peak SiO absorption at 60, 53 and 27 km s^{-1} over a $4'' \times 3.5''$ area covering the UCHII peak at 7 mm. The resulting SiO optical depths and column densities are given in Table 4. We follow Carral & Welch (1992) in assuming a temperature of 2.73 K, which gives a conversion factor of optical depth to column density of 4.2×10^{12} cm^{-2} K km s^{-1}. Carral & Welch gave no HCO$^+$ column density for the 60 km s^{-1} absorption as all the continuum was absorbed, so we have no SiO abundance estimate for that velocity.

The [SiO]/[HCO$^+$] abundances are 0.1 and 0.02 for the 27 and 53 km s^{-1} absorptions respectively, or, assuming X(HCO$^+$) $= 2 \times 10^{-9}$, [SiO]/[H$_2$] $= 0.4$–2×10^{-10}.

We also compared the SiO column density in absorption with the total column density towards the UCHII region estimated from the far infrared optical depth. Campbell et al. (2000) estimate 20.6 micron optical depth of 4.4 for the foreground absorbing clouds. Assuming the optical properties of Draine & Lee (1984), this corresponds to an H$_2$ column density of 10^{23} cm^{-2}. The 9.7 micron silicate absorption feature along the line of sight towards G34.26 has an optical depth of 11.2, corresponding to a column density of 2×10^{23} cm^{-2}, again assuming Draine & Lee optical properties (Faison et al. 1998). Using these hydrogen column density estimates we calculate an SiO abundance of 0.3–0.7×10^{-10}.

These values for the SiO abundance for spiral arm clouds are in agreement with the results for four clouds along the the Sgr B2 and W49 A lines of sight, for which Greaves et al. (1996) derived values of a few times 10^{-11} to 10^{-10}. The results are also in agreement with Greaves & Nyman (1996) who obtain [SiO]/[HCO$^+$] $= 0.02$–0.2 for clouds on the line of sight to Sgr B2(M) (although their [SiO]/[H$_2$] abundance estimates are $\sim10^{-9}$, because they use a larger HCO$^+$ abundance of 1.5×10^{-8}). SiO abundances of $\sim10^{-10}$ are also derived for the more diffuse clouds seen along the line of sight towards extragalactic sources, for which [SiO]/[HCO$^+$] $= 0.01$–0.1 (Lucas & Liszt 2000).

The absorption component which peaks at 60 km s^{-1} is probably due to local gas in the G34.26 molecular cloud as its velocity is close to the 58 km s^{-1} ambient velocity. In absorption this feature has a total column density of 6×10^{12} cm^{-2}, integrating over 56–70 km s^{-1}. From modelling the infrared spectrum, Campbell et al. (2000) estimate a 20.6 micron optical depth of 3×10^{-2} for gas associated with the UCHII region. This corresponds to a column density of $N_{\rm H_2} = 3 \times 10^{21}$ cm^{-2}, and, assuming that this is the gas which we see as the 60 km s^{-1} absorption feature, a SiO abundance of 2×10^{-9}. This is enhanced over the quiescent cloud abundances of $\sim10^{-10}$ and suggests that close to the UCHII shocks may be enhancing the SiO abundance. However, this abundance is uncertain and the mass of gas involved is small.

The column density in the ambient gas in emission (Sect. 3.2) is at least five times as great ($>3 \times 10^{13}$ cm^{-2}). This shows that the material responsible for the ambient velocity SiO emission does not cross in front of the cometary UCHII region C.

4. Conclusions

Towards the high mass star formation region G34.26+0.15, we have observed the shock tracer SiO with the VLA at 43 GHz and in higher transitions with FCRAO and the JCMT. The results are as follows.

– There is a massive blueshifted outflow to the northwest of the ultracompact HII regions. The extent of the outflow is at least 0.6 pc, and its mass is $\sim150\ M_\odot$. The driving source of the outflow is not the main ultracompact HII region C. The UCHII B is a good candidate for the driving source, as it lies on the outflow axis, is deeply embedded (and therefore young) and has the spectral index of a stellar wind. No direct evidence for a

strong SiO abundance enhancement in the outflow was found but moderate enhancements of $X(\mathrm{SiO}) \sim 10^{-8}$ are consistent with the data, if the SiO is clumpy. SiO enhancement at this level can be explained either by slow (<30 km s^{-1}) shocks or by chemical reprocessing and freezeout of SiO reducing previously higher abundances;
- To the southeast and northeast of the UCHII regions are two more areas where SiO is strongly detected. These may be tracing interactions between winds from UCHII B and C and nearby molecular clumps;
- SiO at ambient cloud velocities is widespread across the region, extending over 0.5 pc. From its morphology, this appears to be related to outflow activity and not simply tracing the ambient molecular cloud. SiO abundances for this component are consistent with spiral arm values of $\sim 10^{-10}$, or at most enhanced by a factor of 10;
- We derive a SiO abundance of $[\mathrm{SiO}]/[\mathrm{H_2}] = 0.4\text{–}2\ 10^{-10}$ in Galactic spiral arm molecular clouds which appear as absorption features along the line of sight;
- Either SiO is not strongly enhanced in the hot core, $X(\mathrm{SiO}) < 10^{-8}$, which is consistent with thermal desorption of grains or low shock velocities which remove grain ices, or the column density in the hot core is low, a few times 10^{23} cm^{-2}.

Acknowledgements. The authors would like to thank Michael Rupen at the AOC Socorro for making the VLA observations a success; Mark Thompson for the 450 μm continuum map; Chris Phillips for useful discussions about the nature of UCHII B; and the referee M. Hogerheijde for constructive comments. This work was supported by PPARC grants to the Astrophysics Group at UMIST.

References

Akeson, R. L., & Carlstrom, J. 1996, ApJ, 470, 528
Avery, L. W., & Chiao, M. 1996, ApJ, 463, 642
Bergin, E. A., Neufeld, D. A., & Melnick, G. J. 1998, ApJ, 499, 777
Cabrit, S., & Bertout, C. 1992, A&A, 261, 274
Campbell, M. F., Garland, C. A., Deutsch, L. K., et al. 2000, ApJ, 536, 816
Carral, P., & Welch, W. J. 1992, ApJ, 385, 244
Caswell, J. L., Vaile, R. A., Ellingsen, S. P., & Norris, R. P. 1995, MNRAS, 274, 1126
Caswell, J. L., Vaile, R. A., Ellingsen, S. P., Whiteoak, J. B., & Norris, R. P. 1995, MNRAS, 272, 96
Cesaroni, R., Felli, M., Jenness, T., Neri, R., et al. 1999, A&A, 345, 949
Churchwell, E., Walmsley, C. M., & Cesaroni, R. 1990, A&AS, 83, 119
Churchwell, E., Walmsley, C. M., & Wood, D. O. S. 1992, A&A, 253, 541
Codella, C., Bachiller, R., & Reipurth, B. 1999, A&A, 343, 585
Draine, B. T., & Lee, H. M. 1984, ApJ, 285, 89
Faison, M., Churchwell, E., Hofner, P., et al. 1998, ApJ, 500, 280
Fey, A. L., Spangler, S. R., & Cordes, J. M. 1991, ApJ, 372, 132
Fey, A. L., Gaume, R. A., Nedoluha, G. E., & Claussen M. J. 1994, ApJ, 435, 738
Forster, J. R., & Caswell, J. L. 1999, A&AS, 137, 43
Garay, G., & Rodriguez, L. F. 1990, ApJ, 362, 191
Gaume, R. A., Fey, A. L., & Claussen, M. J. 1994, ApJ, 432, 648
Greaves, J. S., & Nyman, L.-A. 1996, A&A, 305, 950
Greaves, J. S., Ohishi, M., & Nyman, L.-A. 1996, A&A, 307, 898
Hatchell, J., Fuller, G. A., Millar, T. J., Thompson, M. A., & Macdonald, G. H. 2000, A&A, 357, 637
Hatchell, J., Thompson, M. A., Millar, T. J., & MacDonald, G. H. 1998, A&AS, 133 29
Heaton, B. D., Little, L. T., & Bishop, L. S. 1989, A&A, 213, 148
Heaton, B. D., Matthews, N., Little, L. T., & Dent, W. R. F. 1985, MNRAS, 217 485
Heaton, B. D., Little, L. T., Yamashita, T., et al. 1993, A&A, 278, 238
Hofner, P., & Churchwell, E. 1996, A&AS, 120, 283
Hofner, P., Wyrowski, F., Walmsley, C. M., & Churchwell, E. 2000, ApJ, 536, 393
Hunter, T. R., Testi, L., Zhang, Q., & Sridharan, T. K. 1999, AJ, 118, 477
Lucas, R., & Liszt, H. S. 2000, A&A, 355, 327
Macdonald, G. H., Gibb, A. G., Habing, R. J., & Millar, T. J. 1996, A&AS, 119, 333
Matthews, N., Little, L. T., Macdonald, G. H., Andersson, M., et al. 1987, A&A, 184, 284
May, P. W., Pineau des Forêts, G., Flower, D. R., et al. 2000, MNRAS, 318, 809
Mehringer, D. M., & Snyder, L. E. 1996, ApJ, 471, 897
Mezger, P. G., Wink, J. E., & Zylka, R. 1990, A&A, 228, 95
Millar, T. J., Macdonald, G. H., & Habing, R. J. 1995, MNRAS, 273, 25
Millar, T. J., MacDonald, G. H., & Gibb, A. G. 1997, A&A, 325, 1163
Ossenkopf, V., & Henning, Th. 1994, A&A, 291, 943
Wyrowski, F., Schilke, P., & Walmsley, C. M. 1999, A&A, 341, 882
Penzias, A. A. 1981, ApJ, 249, 513
Schilke, P., Walmsley, C. M., Pineau des Forêts, G., & Flower, D. R. 1997, A&A, 321, 293
Scoville, N. Z., Yun Min Su, Sanders, D. B., Clemens, D. P., & Waller, W. H. 1987, ApJS, 63, 821
Shepherd, D. S., & Churchwell, E. 1996, ApJ, 457, 267
Sheherd, D. S., Churchwell, E., & Wilner, D. J. 1997, ApJ, 482, 355
Strong-Jones, F. S., Heaton, B. D., & Little, L. T. 1991, A&A, 251, 263
Watt, S., & Mundy, L. G. 1999, ApJS, 125, 143
Wood, D. O. S., & Churchwell, E. 1989, ApJS, 69, 831
Viti, S., & Williams, D. A. 1999, MNRAS, 305, 755
Ziurys, L. M., & Friberg, P. 1987, ApJ, 314, L49